PVA/PANI/rGO ternary electrospun mats as metal-free anti-bacterial substrates†

Sajjad Ghobadi,[a] Shayan Mehraeen,[a] Rokhsareh Bakhtiari,[a] Bahar Shamloo,[a] Veera Sadhu,[b] Melih Papila,[a] Fevzi Çakmak Cebeci*[ab] and Selmiye Alkan Gürsel*[ab]

Successful performance of biocompatible hybrid systems in various biomedical applications such as wound healing patches, and scaffolds for stem cell preparation have been reported. However, relatively poor structural properties and further bacterial infection have been the major drawbacks for their commercialization. In order to improve the antimicrobial property of such structures, transition metals have been previously added to the media. However, the potential risk of metal pollution as well as hardship of processing has put this approach into obsolescence. Herein the ternary polyvinyl alcohol/reduced graphene oxide/polyaniline fibrous nanocomposites, as substitute for transition metal-containing nanocomposites, were prepared *via* electrospinning. The mats' structural properties (*e.g.* rheological, morphological, electrical and mechanical properties) and their antibacterial properties against *E. coli* bacteria cultures after two different treatments (including thermal and acid doping approaches) were systematically investigated. It was shown that in addition to significant structural improvement, an over 80% antibacterial property enhancement in treated mats in comparison to pristine PVA fibers were achieved. Finally the interaction and main effect analyses were used for suggesting the optimum antibacterial specimen conditions.

Introduction

As well-known 2D materials for polymer matrix reinforcement, graphene and its functionalized derivatives have drawn noticeable attention from the research community.[1] Among the vast variety of graphene-based substances, thermally reduced graphene oxide (rGO) has been reported to show superior mechanical and electrical properties; nevertheless its reinforcing role in polymer-based structures has also proven it to be a promising candidate for various applications such as devices for renewable energy, supercapacitors, and biocompatible nanocomposites.[1b,2]

In addition to noticeable improvement in electrical, mechanical and morphological properties of polymeric electrospun nanocomposite mats by addition of graphene,[3] antimicrobial property introduction to such hybrid biodegradable systems was reported as a result of graphene incorporation to the media.[2a,b,4] Graphene oxide (GO) or reduced GO (rGO) has the ability to destroy the integrity of bacteria membrane by extracting the phospholipids, leading to an antibacterial effect.[5] Also according to a recent study, antibacterial activity of graphene is due to electron transfer interaction from bacterial membrane to graphene.[4] The latter mechanism of bacteria elimination is often proposed to be more effective by addition of transition metals such as Cu[2a] which results in increase in delocalized electron in the media. Thus, the electron transfer through the bacteria membrane occurs. However, the high risk of transition and heavy metal contamination in biocompatible systems, especially in *in vivo* applications, has been the major drawback of this method.

In this work, order to introduce fibrous reinforcement, polyaniline (PANI) with high electrical conductivity, and mechanical stiffness was added to the hybrid mixture. By preparation *via* multi-layer drop-casting method, significantly high electrical and mechanical properties was reported for its polymer nanocomposites both individually and with presence of graphene derivatives.[6] The other reason to choose PANI as the third compartment of the system is its reliable antimicrobial activity *via* preventing microorganisms to adhere to the biodegradable surface.[7]

The electrospinning approach for preparing nanocomposites with ability of obtaining nanometer-scale nonwoven fibrous structure was shown to be one of the most reliable methods among nanocomposite fabrication techniques for its ease of performance, rapid manufacturing, process flexibility and low cost of assembly.[8] Because of the hardship in homogeneous dispersion of thermally reduced graphite oxide (rGO) obtaining in

[a]*Faculty of Engineering and Natural Sciences, Sabanci University, 34956 Istanbul, Turkey. E-mail: fccebeci@sabanciuniv.edu; selmiye@sabanciuniv.edu*

[b]*Sabanci University Nanotechnology Research and Application Center (SUNUM), Sabanci University, 34956 Istanbul, Turkey*

aqueous solutions, successful electrospinning of high graphene-content suspensions were not previously achieved.[9]

Recently, it has been reported that an operon is responsible for polyvinyl alcohol (PVA) degradation by bacteria which is consisted of three genes; oxidized PVA hydrolase (oph), PVA dehydrogenase (pvaA), and cytochrome c (cytC). PVA is converted to acetic acid eventually and enters the metabolic pathway.[10] In our study, we used PVA as nutrient polymer for *Escherchia coli* (*E. coli*) bacteria. This degradation has been suppressed *via* use of different methods, conventionally including a metal substrate to provide delocalized electrons for reactive agents eliminating the bacteria cultures.[2a,b]

Bacteria behave like mitochondria in terms of energy production. They use electron transfer circuit to produce ATP for vital movement.[11] Any disruption in this respiratory chain would be lethal for the bacteria.

Recently, a graphene film plus an underlying substrate have been introduced to show that an electron-pumping mechanism could lead to ROS (Reactive Oxygen Species) independent oxidative stress to the bacteria. Additionally, graphene oxide (GO) or reduced GO (rGO) has the ability to destroy the integrity of bacteria membrane by extracting the phospholipids, leading to an antibacterial effect.[5]

In this method, conductivity of the underlying substrate is extremely important for viability of the bacteria, since transport of the electron coming from the microbial membrane to the graphene film will not be disturbed otherwise.[4] In our study, we substitute the metal conductive layer with a conducting polymer (PANI), as an extra cellular electron acceptor for bacteria; therefore we prevent any further metal toxicity.

Herein, the effectiveness of co-solvent addition method[3c] in preparation of rGO/PANI dispersions was studied and the rheological behavior of their relative rGO/PANI/PVA ternary suspensions were comprehensively investigated. This investigation provided the required information for modulation of suspension behavior and consistency during the electrospinning, which was probed *via* extensional and rotational rheology analysis. Following the electrospinning, effect of PANI and rGO addition to media on morphological and mechanical properties of as-spun fibers were studied. The effect of two different post-spinning treatments, cross-link/acid doping and thermal treatment, respectively, on electrical and antibacterial properties of the as-spun mats were investigated. To the best of our knowledge the mentioned approach was the first of its kind in order to prepare antibacterial metal-free thin layers.

Experimental methods

Materials

N,*N*-Dimethyl formamide, graphite flakes, polyvinyl alcohol (average M.W. 89 000–98 000 g mol^{-1}), aniline monomer, *p*-phenylenediamine, potassium permanganate ($KMnO_4$), sulphoric acid (H_2SO_4), phosphoric acid (H_3PO_4), hydrochloric acid (HCl), hydrogen peroxide (H_2O_2), and ethanol were purchased from Sigma-Aldrich (Taufkirchen, Germany) and used with no further purification.

Electrospinning

The rGO was prepared based on our synthesis protocol[3c] and PANI nanofibers were prepared *via* the so-called rapid mixing method.[12] Preparation of electrospinning suspensions were conducted based on our co-solvent assisted method[10] for dispersion preparation of rGO and emeraldine-based PANI (PANI-EB) where the final PVA content was kept constant at 12 w/v%.

The prepared electrospinning suspensions were conveyed through and electrospun *via* a 5 mL plastic syringe with flow rate of 3.5 μL min^{-1}. The optimized electric potential difference and the needle tip to the 15×15 cm^2 aluminum foil collector distance were 13 kV and 15 cm, respectively. The electrospun mats were gently peeled off from the foil for further treatment and characterizations.

Post-spinning treatments on PVA/rGO/PANI ternary fibrous mats

In order to cross-link the mats, an approach suggested by Chu and co-workers were pursued.[13] During this process as-spun mats were cross-linked *via* immersion into 0.15 M glutaraldehyde (GA) solution for 1 hour at room temperature. The cross-linked mats were then washed with DI water for excessive glutaraldehyde removal.

The doping was conducted through immersion of the cross-linked mats into the HCl solution for 1 hour at room temperature. Afterwards, the excess acid was removed from the mats *via* washing the doped mats with DI water. Finally, the mats were dried in oven for 24 hours at 50 °C.

Pursuing the goals of partial elimination of the electrically insulating PVA matrix, the thermal treatment was conducted at 220 °C for 10 minutes. The heating rate was 10 °C min^{-1} and the Ar atmosphere was used for this process.

Extensional and rotational viscometry analyses

The extensional viscometry analysis of electrospinning solutions, as an index for electrospinning process, was studied *via* Thermo Scientific Haake-CaBER 1 capillary breakup extensional rheometer. Additionally, the behavioral deviation of suspensions from the Newtonian was studied *via* an Anton Paar MCR 302 rotational rheometer device. The detailed analysis on the results of the rheological properties can be found in the ESI.†

Scanning and transmission electron microscopy

SEM imaging from the exterior texture of specimens was conducted *via* a Zeiss Leo supra 35VP SEM-FEG. For this analysis samples were sputter coated using a gold target. The images obtained were further analyzed by Image J software for statistical study on average fiber diameters as well as bacteria population investigation.

The interior morphology of ternary nanocomposite mats was investigated by a Jeol 2000FX TEM system. The results were then used for detection of rGO and PANI nanoparticles and locating their position inside the fibrous structure.

FT-IR analysis

In order to confirm the cross-linking of the samples *via* different approaches as well as to study the doping of incorporated PANI, the specimens were subjected to a Fourier transformed-IR spectroscopy analysis *via* a Thermo Scientific iS10 FTIR spectroscopy device.

Electrical conductivity measurement

The effect of aforementioned treatment approaches on the electrical conductivity of post-spinning treated samples were measured *via* a CR-Cascade Microtech CP4 4-point probe electrical conductivity measurement device. The results were then investigated for clarification of linear resistance behavior of specimens.

Mechanical behavior

The mechanical properties of as-spun mats was studied by a UTM machine in tension mode. For each sample 5 respective specimens of 1×2.5 cm were prepared. The drawing speed and the grip to grip distance were set at 1 mm min^{-1} and 25 mm, respectively. In this set of experiments a 200N load cell was used. The information on specimen preparation can be found in the ESI† under Section 1.2. In order to compare mechanical properties of graphene-containing samples with the ternary nanocomposites, a 2 wt% graphene-containing sample was prepared for this analysis. The sample was coded as G2P0.

Anti-bacterial analysis

In order to study the antibacterial performance of treated samples, *E. coli* MG1655 cultures. The cultures were grown through the approach proposed by Parra *et al.*[2a] After growing the bacteria in a media with mild ionic strength using meat and yeast extracts both at 5 g L^{-1} concentration. Afterwards, the cultures were concentrated by centrifugation at 5000g for 5 minutes. The final stock dispersion was kept at 109 CFU mL^{-1}.

The samples were put in separate vessels with the concentrated bacteria cultures and incubated at 37 °C for 24 hours in a humidity chamber followed by centrifugation of samples in DI water at 3000g for 3 minutes to remove the free bacteria fraction that did not adhered to the surface. In order to study the specimens *via* SEM, the adhered bacteria culture was stabilized by 1 v/v% glutaraldehyde aqueous solution. The *E. coli* population adhered to the specimen surfaces was then calculated using Image J software from their respective SEM images. For the sake of convenience, during this study the cross-linked and the thermally treated samples were coded as "C" and "T", respectively. For each case, 5 trials were investigated and average results were reported.

In order to show the significance of each factor, main effect and interaction effect statistical analyses were conducted on the antibacterial trials results *via* Minitab® 17.0 software. The treatment type, PANI, and rGO content were the factors studied. Detailed information regarding the statistical analyses are presented in ESI.†

Results and discussion

Table 1 shows that three levels of concentration for each of the filler materials (rGO and PANI) was considered in the design.

Morphology study of ternary electrospun mats

The SEM images of the sample only containing PANI (Fig. 1A) showed a ribbon-like fiber texture. This specific formation of the fibers has been reported to be due to formation of PANI percolation network, making entrapping the water inside the suspension jet. Thus the drying of the electrospun fibers was interfered resulting in structure collapse.[14] Thus the ribbon-like PANI/PVA nanocomposites was formed. The addition of rGO to the electrospinning suspension resulted in more robustness in the electrospun fibers. As a result the 3D fibrous shape of fibers

Table 1 Material composition of ternary electrospun mats planned for conductivity study

Sample	rGO content (*ca.* wt% in dry media)	PANI content (*ca.* wt% in dry media)
G0P1	0	1
G0P2.5	0	2.5
G0P4[a,b]	0	4
G1P1	1	1
G1P2.5	1	2.5
G1P4[b]	1	4
G2P1	2	1
G2P2.5	2	2.5
G2P4[a,b]	2	4

[a] Screening of mechanical behavior. [b] Screening of rheological behavior.
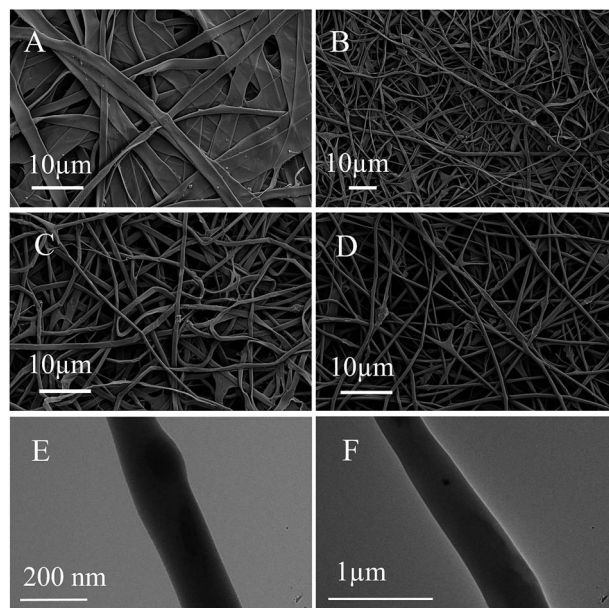

Fig. 1 SEM images of samples (A) G0P1, (B) G1P1, (C) G1P4, (D) G2P4, and TEM images of (E) G0P4 and (F) G2P4.

was kept intact during the drying leading to obtain fiber textures for the mentioned samples (Fig. 1B–D). The trend of morphology change was also complementing the material composition change throughout the samples. As the rGO content was increased from 1 wt% in G1P4 sample to 2 wt% in G2P4 (Fig. 1C and D, respectively) the fibrous textures was increased while the 2D ribbon-like structure was extensively reduced.

In the TEM images of G0P4 sample (Fig. 1E), the formation of filler agglomerates within the electrospun fibers, with various shapes and sizes, can be observed. For example a spherical agglomeration of particles was recorded in the sample's TEM image. Formation of structures containing various compositions of embedded PANI and rGO was regarded as a result of high conductive polymer content within the nanocomposite composition and the relative fluctuations added to the spinning process accordingly.[15]

A noticeable change in the diversity of filler structure types recorded in G2P4 sample (Fig. 1F) in comparison with the one with no added rGO filler was observed during the transmission electron microscopy. Addition of another filler material (rGO) with extremely high mechanical and electrical properties resulted in an increase in the fiber diameter as well as formation of different filler cluster formations, and placement within the as-spun fibrous nanocomposite. Since PANI nanofibers had stronger interactions with the hydrophilic matrix, their agglomerates were found to be larger, while the rGO clusters showed lower dimensions. Such type of aggregation in the rGO nanoparticles was a result of low affinity between hydrophilic matrix and hydrophobic filler material.[16]

Although the existence of PANI clusters inside the ternary nanofibers were confirmed *via* other characterization analyses shown later on, the TEM imaging was not able to detect the exact morphology of PANI network agglomerations after further treatments.

Mechanical properties analysis

The stress–strain curves (representative samples in Fig. 2A) show a consistent general behavior under applied tension load. However, the strain at break was significantly reduced with respect to the increase in fillers (rGO and PANI) contents where for G2P4 sample the strain at break was over 30% lower than the pristine sample. This phenomenon was reported before as lowering individual fiber necking due to presence of low-strain filler materials.[3c]

The tensile strength analysis on the drawn samples (Fig. 2B) showed that this value was increased with respect to high strength filler addition and the trend was shown consistency through the whole data set which it was ultimately reached to 3.67 MPa to be over 40% higher than the pristine sample. Although increase in weak filler–filler interactions in high filler-content samples such as G0P4 and G2P4 samples was expected to result in a decrease in the tensile strength of the samples,[3c] the percolation network formed by the PANI and its interaction with rGO nanosheets, led to strength values even higher than the G2P0 sample only reinforced by graphene nanosheets.[3a,c,17]
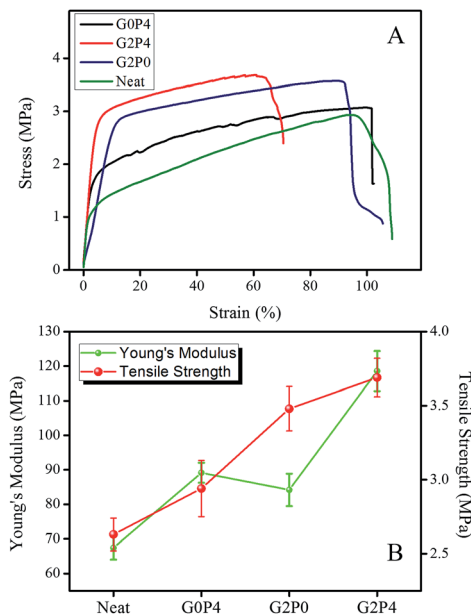

Fig. 2 (A) Stress–strain, (B) tensile strength, and Young's modulus graphs of selected samples.

While studying the Young's modulus of the samples (Fig. 2B), an almost two times-fold increase in this property was achieved for rGO/PANI reinforced fibers in comparison with the neat PVA mats. This observation was due to desirable filler materials dispersion achievement thus increasing the filler–polymer interactions in the system.

This phenomenon resulted in improvement in formation of desirable dispersion of additive materials leading to increase in material stiffness. However, the only-graphene containing sample (G2P0) did not follow the mentioned trend of behavior which was due to lack of a percolation network of PANI within its fibrous structure. This resulted in lower Young's modulus in the latter sample.

Post-spinning treatment analysis

Cross-linking/acid doping. In order to be able to re-dope the incorporated PANI with an aqueous acidic solution, to transform it into emeraldine salt conductive state, a cross-linking step was needed to be performed on the as-spun mats. As it was shown in Fig. 2B the fibers cross-linked with GA demonstrate a noticeable change in texture during which the fibers start to merge into each other and form an inter-connected network. This effect not only improves the mechanical stiffness of prepared mats but also aids the nanocomposite with better contact of embedded PANI and rGO particles among each other. These improvements further enhanced the quality of obtained fibrous nanocomposite in terms of mechanical, electrical, and thermal properties.[8b,13]

Successful cross-linking of the as-spun mats was confirmed by the FT-IR spectroscopy in which the definitive peaks for covalent bonds formed during the process were detected. Within the Fig. 3, by focusing on detection of the peaks for PVA and GA bonds, at 1085–1150, 1735–1750, 2695–2830, and 3200–
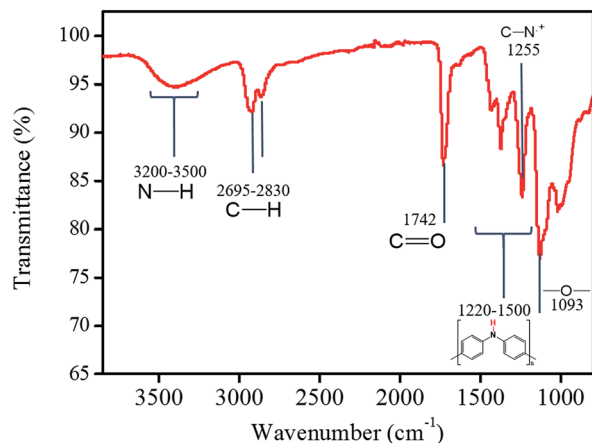
Fig. 3 FT-IR spectrum of cross-linked and acid-doped sample (G1P1).

Fig. 4 (A) FT-IR spectrum, (B) TGA and DTG analysis of thermally treated sample (G1P2.5).

3550 cm^{-1} ranges the ether, carboxylic, aldehyde double-peaks, and a broad amine group peak between PVA and GA was detected, respectively.[6,18] Thus the successful formation of cross-linking covalent bonds was confirmed by this analysis.

Additionally, the relative peaks indicating the incorporation of PANI in the nanocomposite structure was also detected. According to IUPAC technical report,[19] emeraldine salt form of PANI showed multiple peaks at $1550–1240 \text{ cm}^{-1}$. The 1481, 1307, and 1255 cm^{-1} picks represented the benzenoid structure, the C–N of secondary amine groups, and the $C–N^+$ stretching in the polaron structure of PANI, respectively. Therefore, the confirmation on incorporation of PANI nanofibers was successfully achieved *via* this study. However, since the vibrational intensity of EB-PANI was low, the determining peak of PANI's form, at $1750–1650 \text{ cm}^{-1}$ range indicating the PANI quinoid structure[20] was covered by high-intensity PVA and PVA-GA covalent bonds' background. Additionally the broad $3200–3500 \text{ cm}^{-1}$ peak was the indication for the N–H stretching of amine groups including the amine groups found in the EB-PANI structure.[13,18]

Thermal treatment. TGA analysis as an index of thermal treatment process was conducted on the samples. During the process, which was kept identical to the treatment conditions, a heating ramp followed by the isothermal step all under neutral gas constant purge was executed (Fig. 4B). In the respective TGA graph of the experiment it was shown that after a dehydration step at around 100 °C, the mass loss didn't continue until the starting point of the isothermal step at 220 °C. At that region a graph shape was transformed into a decreasing trend behavior indicating the decomposition of PVA matrix. Despite the extensive volume change of as-spun mats after the treatment, both the TGA and FTIR results indicate that most of the matrix fraction remains intact even during the isothermal heating step as the over 95% remaining mass, and high intensity PVA backbone IR peaks was shown, respectively.[21]

The FT-IR spectroscopy results obtained from thermally treated samples showed two main desired characteristics achieved by means of such a treatment approach. Firstly, a mild cross-link of PVA matrix was ac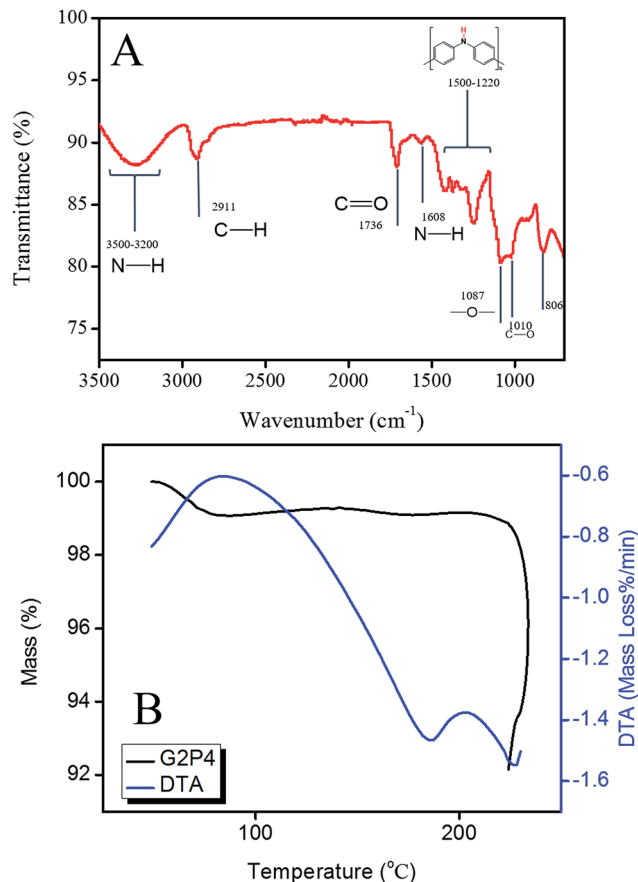hieved and this is due to detection of inter-chain bond peaks at 2911, 1700–1750, and 1010 cm^{-1} ranges, through which the presence of the C–H stretching bonds in alkyl groups, C=O, and C–O stretching in crystalline PVA was confirmed, respectively.[18,22] As the second remark of this analysis, desirable thermal doping of PANI through thermal treatment was also validated. The generic PANI multiple peaks at $1500–1250 \text{ cm}^{-1}$ range,[19,20] discussed in the previous section, as well as the 806 cm^{-1} benzenoid structure peak was detected. As the target of the study, the specific peak for emeraldine salt (ES) form among all of the states of PANI, at 1608 cm^{-1}, indicating the N–H scissoring of the primary aromatic amine groups,[19,20] was reported in the spectrum. The mentioned peak had a low intensity that also matched the previous results of PANI spectroscopy analysis in which the intensity of the spectrum peaks were low (Fig. 4A).[18,23]

Electrical conductivity analysis

The electrical conductivity measurement on ternary mats pre-treatment showed no sign of conductivity despite having electrically conductive additives in their structure.

The effect of increase in rGO content was demonstrated to be the key factor in the electrical conductivity of the samples. By following the trend of sample composition change in Table 2, it can be seen that regardless of PANI amount, after each of 1%

rGO content-increase levels, the electrical conductivity of samples had reached to at least an order of magnitude higher values compared to samples of previous steps. This phenomenon was shown to be the result of both extremely higher conductivity and specific surface area values of rGO compared to PANI nanofibers, resulting in a noticeable improvement in measured electrical conductivity of the samples. The higher surface area graphene also provides a better distribution of PANI as well as enhanced connection of fillers between each other, thus the increase in electrical properties was achieved.[14b,23]

While based on the trend of the change in properties it was expected that the sample with highest amount of conductive fillers (G2P4) should show the best performance, the sample containing one level lower amount of PANI had better records in conductivity values by over a time fold comparing the high concentration sample.

In the G2P4 sample, the properties were affected by lack of desired filler exfoliation and homogeneous distribution throughout the nanocomposite, further resulting in formation of filler island-like agglomerations along the as-spun fibers. The occurrence of such structures was confirmed earlier by TEM imaging of the mentioned sample (Fig. 1F).

On the contrary by setting the G2P2.5 sample material composition as such, not only high amount of conductive fillers were provided to the electrospinning solution but also the possibility of achieving a more homogeneous dispersion of PANI and rGO in the initial co-solvent by keeping the PANI concentration at the moderate level of 2.5 wt% rather than increasing to higher levels. The well-dispersed distribution of PANI nanofibers was also aided by rGO nanolayers with high available surface area, further improving the network of conductive filler material within this specific nanocomposite structure.[23]

Electrical conductivity values of thermally treated samples reported in Table 2 showed that the conductivity property of graphene containing samples were at least three orders of magnitude higher than those only contain PANI as their conductive additive material. Such further increase in electrical properties was mainly regarded as a result of partial elimination of the insulating PVA matrix due to the mild thermal treatment.[23] The other effective result of the mentioned neutral gas calcination was the merging of electrospun fibers while the filler

network remained intact and also the probability of formation of a percolation among networks of fillers in separate electrospun fibers was increased. Formation of a percolation network of fillers embedded inside the nanocomposite was the responsible factor in the general increase in the thermally treated samples' electrical properties in comparison with the acid-doped trials (Table 2).

As a similar case of study it was shown that the electrical conductivity has undergone a limited amount of increase with respect to the increase in PANI content at each of the graphene content levels (Table 2). The range of increase in the studied electrical properties between different rGO concentration-levels are more noticeable where the electrical conductivity of 3 nS cm^{-1} in G0P1 sample was increased up to 19.06 μS cm^{-1} at G2P1 sample.

This study suggested that since the cross-link/acid doping results showed a more reliable trend of electrical conductivity improvement, the mentioned approach would be a favorable route for electrical conductivity improvement compared to the thermal treatment approach. However, during the investigation, the highest electrical conductivity value was achieved by the latter approach.

Anti-bacterial analysis

The bacteria elimination was conducted through two different mechanisms. On one hand, the incorporated PANI prevented the adhesion of bacteria so that the cultures of the organism could not be formed and the PVA structure was kept intact.[7a,c] On the other hand, the rGO nanosheets showed antibacterial effect on the adhered *E. coli* through the proven mechanism of destroying the bacteria membrane integrity by extraction of phospholipids without interfering in the electron transfer chain of the bacteria *via* metal introduction into the system.[2a,b,4,5]

The treatment type had a major effect on the bacteria culture suppression behavior of as-spun mats. The SEM imaging followed by statistical analysis of the thermally treated samples [Fig. 5D and E] showed that although antibacterial additive materials had a desired percolation network, their network was completely surrounded by the PVA due to melting and turning the mat's porous structure into a bulk material. While for the acid/doped samples [Fig. 5B and C] as the porous structure was kept intact, the incorporated PANI and rGO with identical contents were more effective in elimination of the bacteria. Thus the culture suppression recorded for thermally treated samples was over two times fold higher compared to the acid-doped specimens.

Although no electron-providing metal component was used in these thin films, the significant improvement in bacterial culture suppression indicated the successful preparation of all-organic antibacterial where in Fig. 5F it was shown that the population of *E. coli* was suppressed from 626 mm^{-1} in the pristine PVA sample to 98 mm^{-1} in CG2P4 sample (Fig. 5C) which was assisted by both of the elimination mechanisms. The significant 80% decrease in adhered bacteria population was slightly lower for CG2P0 indicating that the destruction of the

Table 2 Electrical conductivity of cross-linked/acid-doped samples

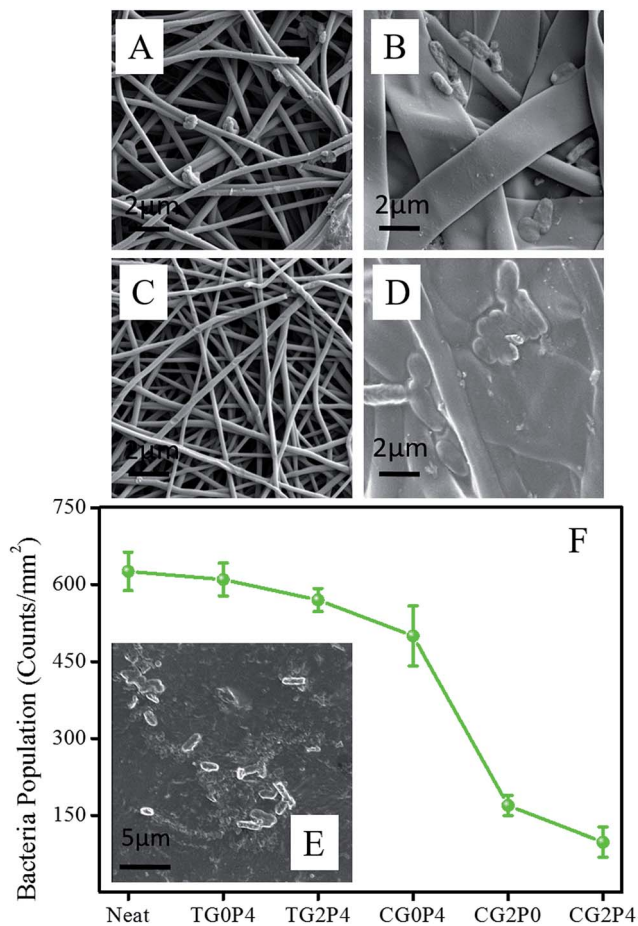| Sample	Acid treatment conductivity (μS cm^{-1})	Thermal treatment conductivity (μS cm^{-1})
G0P1	0.004 ± 0.001	0.03 ± 0.001
G0P2.5	0.005 ± 0.002	0.06 ± 0.001
G0P4	0.023 ± 0.009	0.03 ± 0.01
G1P1	0.33 ± 0.01	0.14 ± 0.01
G1P2.5	0.74 ± 0.012	0.7 ± 0.008
G1P4	1.51 ± 0.01	1.3 ± 0.06
G2P1	6.84 ± 0.05	19.06 ± 0.11
G2P2.5	14.41 ± 0.24	4.83 ± 0.38
G2P4	6.41 ± 0.1	11.54 ± 0.1

Fig. 5 SEM images of (A) neat, (B) CG0P4, (C) CG2P4, (D) TG0P4, (E) TG2P4, and (F) bacteria population graph of specimens.

Conclusion

Through systematic analysis of nonwoven ternary rGO/PANI/PVA mats it was shown that significant properties improvements were achieved through addition of the rGO nanosheets as well as PANI nanofibers to the pristine PVA mats.

In order to improve the electrical conductivity as well as enabling the mats to effectively react to the bacteria culture exposure two different treatments, crosslink/acid doping, and thermal treatment, were applied to the as-spun mats. It was shown that the electrical conductivity of the samples was significantly improved through both of the treatments. Though the tuning ability of the crosslink/acid doping approach was shown to be more promising.

The electron microscopy and bacteria population analysis of the treated mats after exposure to *E. coli* bacteria cultures was conducted and statistically studied as well. It was shown that the addition of rGO and PANI additives improved the antibacterial properties of the mats compared to the neat samples. The noticeable enhancement of the antibacterial activity reached its peak while the ternary mats were treated *via* crosslink/acid doping method. It was shown that through this approach, the initial porous morphology of the mats were kept intact, thus enabling the effective interaction between the additives and bacteria culture. Finally the optimized conditions to achieve the highest antibacterial properties also was suggested.

Acknowledgements

Notes and references

1 (*a*) W. Yuan, L. Huang, Q. Zhou and G. Shi, Ultrasensitive and Selective Nitrogen Dioxide Sensor Based on Self-Assembled Graphene/Polymer Composite Nanofibers, *ACS Appl. Mater. Interfaces*, 2014, **6**(19), 17003–17008; (*b*) B. Yu, Y. Shi, B. Yuan, S. Qiu, W. Xing, W. Hu, L. Song, S. Lo and Y. Hu, Enhanced thermal and flame retardant properties of flame-retardant-wrapped graphene/epoxy resin nanocomposites, *J. Mater. Chem. A*, 2015, **3**(15), 8034–8044; (*c*) J. Huang, H. Deng, D. Song and H. Xu, Electrospun polystyrene/graphene nanofiber film as a novel adsorbent of thin film microextraction for extraction of aldehydes in human exhaled breath condensates, *Anal. Chim. Acta*, 2015, **878**, 102–108.

2 (*a*) C. Parra, F. Montero-Silva, R. Henríquez, M. Flores, C. Garín, C. Ramírez, M. Moreno, J. Correa, M. Seeger and P. Häberle, Suppressing Bacterial Interaction with Copper Surfaces through Graphene and Hexagonal-Boron Nitride Coatings, *ACS Appl. Mater. Interfaces*, 2015, **7**(12), 6430–6437; (*b*) P. Subramanian, F. Barka-Bouaifel, J. Bouckaert,

bacteria membrane had the stronger effect as the only counter agent in the later sample was rGO. This evaluation was also supported by the analysis on the CG0P4 sample with no incorporated graphene nanosheets. Study showed that only the limited 30% decrease in population was recorded in that sample in comparison with the neat one.

It is also worth to note that since the thermally treated sample fibers were merged into each other, the effective exposure to the additive materials was blocked by PVA film. However, in acid doped samples the porous structure of mats were kept intact resulting in a more effective interaction between rGO and PANI with the bacteria culture. Thus superior antibacterial activity of acid doped samples compared to the thermally treated trials can be explained from the morphological point of view.

The statistical analysis on the antibacterial property investigation (see ESI†) also confirmed that the most effective antibacterial properties were achieved through cross-linking/acid doping method, and *via* using the highest amount of additive agents, respectively. As a result the CG2P4 sample antibacterial thin film is suggested have the performance among the trials prepared *via* the proposed thin film fabrication system.

N. Yamakawa, R. Boukherroub and S. Szunerits, Graphene-Coated Surface Plasmon Resonance Interfaces for Studying the Interactions between Bacteria and Surfaces, *ACS Appl. Mater. Interfaces*, 2014, **6**(8), 5422–5431; (*c*) L. Kyhl, S. F. Nielsen, A. G. Cabo, A. Cassidy, J. A. Miwa and L. Hornekaer, Graphene as an anti-corrosion coating layer, *Faraday Discuss.*, 2015, **180**, 495–509; (*d*) D. A. Oriero, J. M. F. Jabal, L. Deobald, A. T. Weakley and D. E. Aston, A potential enzyme-encapsulating, ultrafine fiber for phenol detection, *React. Funct. Polym.*, 2011, **71**(8), 870–880.

3 (*a*) S. Panzavolta, B. Bracci, C. Gualandi, M. L. Focarete, E. Treossi, K. Kouroupis-Agalou, K. Rubini, F. Bosia, L. Brely, N. M. Pugno, V. Palermo and A. Bigi, Structural reinforcement and failure analysis in composite nanofibers of graphene oxide and gelatin, *Carbon*, 2014, **78**, 566–577; (*b*) F. Barzegar, A. Bello, M. Fabiane, S. Khamlich, D. Momodu, F. Taghizadeh, J. Dangbegnon and N. Manyala, Preparation and characterization of poly(vinyl alcohol)/graphene nanofibers synthesized by electrospinning, *J. Phys. Chem. Solids*, 2015, **77**, 139–145; (*c*) S. Ghobadi, S. Sadighikia, M. Papila, F. C. Cebeci and S. Alkan Gursel, Graphene-reinforced Poly(vinyl alcohol) Electrospun Fibers as Building Blocks for High Performance Nanocomposites, *RSC Adv.*, 2015.

4 J. Li, G. Wang, H. Zhu, M. Zhang, X. Zheng, Z. Di, X. Liu and X. Wang, Antibacterial activity of large-area monolayer graphene film manipulated by charge transfer, *Sci. Rep.*, 2014, **4**, 4359.

5 Y. Tu, M. Lv, P. Xiu, T. Huynh, M. Zhang, M. Castelli, Z. Liu, Q. Huang, C. Fan, H. Fang and R. Zhou, Destructive extraction of phospholipids from *Escherichia coli* membranes by graphene nanosheets, *Nat Nano*, 2013, **8**(8), 594–601.

6 T. Mosciatti, S. Haar, F. Liscio, A. Ciesielski, E. Orgiu and P. Samorì, A Multifunctional Polymer-Graphene Thin-Film Transistor with Tunable Transport Regimes, *ACS Nano*, 2015, **9**(3), 2357–2367.

7 (*a*) M. Ghaffari-Moghaddam and H. Eslahi, Synthesis, characterization and antibacterial properties of a novel nanocomposite based on polyaniline/polyvinyl alcohol/Ag, *Arabian J. Chem.*, 2014, **7**(5), 846–855; (*b*) L. E. Ibarra, L. Tarres, S. Bongiovanni, C. A. Barbero, M. J. Kogan, V. A. Rivarola, M. L. Bertuzzi and E. I. Yslas, Assessment of polyaniline nanoparticles toxicity and teratogenicity in aquatic environment using *Rhinella arenarum* model, *Ecotoxicol. Environ. Saf.*, 2015, **114**, 84–92; (*c*) S. H. Kim, E. B. Kang, C. J. Jeong, S. M. Sharker, I. In and S. Y. Park, Light Controllable Surface Coating for Effective Photothermal Killing of Bacteria, *ACS Appl. Mater. Interfaces*, 2015, **7**(28), 15600–15606.

8 (*a*) J. Wang, X. Zhao, J. Li, X. Kuang, Y. Fan, G. Wei and Z. Su, Electrostatic Assembly of Peptide Nanofiber–Biomimetic Silver Nanowires onto Graphene for Electrochemical Sensors, *ACS Macro Lett.*, 2014, **3**(6), 529–533; (*b*) S. Kim, P. Zhao, S. Aikawa, E. Einarsson, S. Chiashi and S. Maruyama, Highly Stable and Tunable n-Type Graphene Field-Effect Transistors with Poly(vinyl alcohol) Films, *ACS*

Appl. Mater. Interfaces, 2015, **7**(18), 9702–9708; (*c*) L. P. Biro, P. Nemes-Incze and P. Lambin, Graphene: nanoscale processing and recent applications, *Nanoscale*, 2012, **4**(6), 1824–1839.

9 K. Fujikura, S. Lin, J. Nakamura, A. Obata and T. Kasuga, Preparation of electrospun fiber mats using siloxane-containing vaterite and biodegradable polymer hybrids for bone regeneration, *J. Biomed. Mater. Res., Part B*, 2013, **101**(8), 1350–1358.

10 X. Hu, R. Mamoto, Y. Fujioka, A. Tani, K. Kimbara and F. Kawai, The PVA operon is located on the megaplasmid of *Sphingopyxis* sp. strain 113P3 and is constitutively expressed, although expression is enhanced by PVA, *Appl. Microbiol. Biotechnol.*, 2008, **78**(4), 685–693.

11 H. W. Harris, M. Y. El-Naggar, O. Bretschger, M. J. Ward, M. F. Romine, A. Y. Obraztsova and K. H. Nealson, Electrokinesis is a microbial behavior that requires extracellular electron transport, *Proc. Natl. Acad. Sci. U. S. A.*, 2010, **107**(1), 326–331.

12 J. Huang, S. Virji, B. H. Weiller and R. B. Kaner, Polyaniline Nanofibers: Facile Synthesis and Chemical Sensors, *J. Am. Chem. Soc.*, 2003, **125**(2), 314–315.

13 Y. Liu, R. Wang, H. Ma, B. S. Hsiao and B. Chu, High-flux microfiltration filters based on electrospun polyvinylalcohol nanofibrous membranes, *Polymer*, 2013, **54**(2), 548–556.

14 (*a*) Q. Du, D. R. Harding and H. Yang, Helical peanut-shaped poly(vinyl pyrrolidone) ribbons generated by electrospinning, *Polymer*, 2013, **54**(25), 6752–6759; (*b*) K. Sujith, A. M. Asha, P. Anjali, N. Sivakumar, K. R. V. Subramanian, S. V. Nair and A. Balakrishnan, Fabrication of highly porous conducting PANI-C composite fiber mats *via* electrospinning, *Mater. Lett.*, 2012, **67**(1), 376–378.

15 S. Wu, Q. He, C. Tan, Y. Wang and H. Zhang, Graphene-Based Electrochemical Sensors, *Small*, 2013, **9**(8), 1160–1172.

16 (*a*) P. Frontera, C. Busacca, P. Antonucci, M. L. Faro, E. Falletta, C. D. Pina and M. Rossi, Polyaniline nanofibers: towards pure electrospun PANI, *AIP Conf. Proc.*, 2012, **1459**(1), 253–255; (*b*) S. S. Qavamnia and K. Nasouri, Conductive polyacrylonitrile/polyaniline nanofibers prepared by electrospinning process, *Polym. Sci., Ser. A*, 2015, **57**(3), 343–349.

17 X. Xu, A. J. Uddin, K. Aoki, Y. Gotoh, T. Saito and M. Yumura, Fabrication of high strength PVA/SWCNT composite fibers by gel spinning, *Carbon*, 2010, **48**(7), 1977–1984.

18 H. S. Mansur, C. M. Sadahira, A. N. Souza and A. A. P. Mansur, FTIR spectroscopy characterization of poly(vinyl alcohol) hydrogel with different hydrolysis degree and chemically crosslinked with glutaraldehyde, *Mater. Sci. Eng., C*, 2008, **28**(4), 539–548.

19 M. Trchová and J. Stejskal, Polyaniline: the infrared spectroscopy of conducting polymer nanotubes (IUPAC Technical report), *Pure Appl. Chem.*, 2011, **83**(10), 1803–1817.

20 A. Yelil Arasi, J. Juliet Latha Jeyakumari, B. Sundaresan, V. Dhanalakshmi and R. Anbarasan, The structural

properties of poly(aniline)—analysis *via* FTIR spectroscopy, *Spectrochim. Acta, Part A*, 2009, **74**(5), 1229–1234.

21 F. Wang, X. Xu, J. Gong, Y. Luo, Y. Hou, X. Zheng and L. Qu, Polyaniline microrods synthesized by a polyoxometalates/ poly(vinyl alcohol) microfibers template, *Mater. Lett.*, 2005, **59**(29–30), 3982–3985.

22 S.-Y. Lin, W.-T. Cheng, Y.-S. Wei and H.-L. Lin, DSC-FTIR microspectroscopy used to investigate the heat-induced intramolecular cyclic anhydride formation between Eudragit E and PVA copolymer, *Polym. J.*, 2011, **43**(6), 577–580.

23 M. K. Shin, Y. J. Kim, S. I. Kim, S.-K. Kim, H. Lee, G. M. Spinks and S. J. Kim, Enhanced conductivity of aligned PANi/PEO/MWNT nanofibers by electrospinning, *Sens. Actuators, B*, 2008, **134**(1), 122–126.